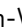





## High efficiency green InP quantum dot light-emitting diodes by balancing electron and hole mobility

Wei-Chih Chao<sup>1</sup>, Tzu-Hsuan Chiang<sup>1</sup>, Yi-Chun Liu<sup>1</sup>, Zhi-Xuan Huang<sup>1</sup>, Chia-Chun Liao<sup>2</sup>, Chen-Hsien Chu<sup>2</sup>, Chih-Hsing Wang<sup>1</sup>, Huan-Wei Tseng<sup>2</sup>, Wen-Yi Hung<sup>3</sup> & Pi-Tai Chou<sup>1</sup>

The industrialization of quantum dot light-emitting diodes (QLEDs) requires the use of less hazardous cadmium-free quantum dots, among which ZnSe-based blue and InP-based green and red quantum dots have received considerable attention. In comparison, the development of InP-based green QLEDs is lagging behind. Here, we prepare green InP/ZnSe/ZnS quantum dots with a diameter of 8.6 nm. We then modify the InP quantum dot emitting layer by passivation with various alkyl diamines and zinc halides, which decreases electron mobility and enhances hole transport. This, together with optimizing the electron transport layer, leads to green 545 nm InP QLEDs with a maximum quantum efficiency (EQE) of 16.3% and a current efficiency 57.5 cd/A. EQE approaches the theoretical limit of InP quantum dots, with an emission quantum yield of 86%.

<sup>1</sup>Department of Chemistry, National Taiwan University, 10617 Taipei, Taiwan. <sup>2</sup>Unique Materials Co., Ltd, Taipei, Taiwan. <sup>3</sup>Department of Optoelectronics and Materials Technology, National Taiwan Ocean University, 20224 Keelung, Taiwan. ✉email: [titan.tseng@unimater.com](mailto:titan.tseng@unimater.com); [wenhung@mail.ntou.edu.tw](mailto:wenhung@mail.ntou.edu.tw); [chop@ntu.edu.tw](mailto:chop@ntu.edu.tw)

Colloidal quantum dots (QDs) are considered as the next-generation emissive materials for quantum light-emitting diodes (QLEDs) owing to their size controllable bandgaps, excellent photoelectric properties and high color purity<sup>1–4</sup>. The first QLED reported in 1994<sup>5</sup> suffered an extremely low external quantum efficiency (EQE) of less than 0.01%. It was not until 2011, a milestone for the breakthrough was made, where QLED was emerged with the introduction of n-type ZnO nanoparticles into the hybrid QLEDs as the electron transport layer (ETL), demonstrating then a high luminance ( $68,000 \text{ cd m}^{-2}$ ) for green CdSe-ZnS QDs<sup>1</sup>. Ever since, progress has been continuously evolved for the CdSe relevant QLEDs, where EQE reaches the theoretical limit of 20% and luminance that attains  $3.6 \times 10^5$ ,  $1.7 \times 10^6$ , and  $6.3 \times 10^4 \text{ cd m}^{-2}$  for red, green, and blue devices, respectively<sup>2,6–11</sup>. Despite excellent performance for CdSe relevant QLEDs, however, the use of Cd has been banned in numerous consumer electronics because of its environment and health hazard<sup>1,2</sup>. In the quest of an alternative, the development of Cd-free QLEDs is thus demanding for their broad and practical implementation. In this regard, QLEDs incorporating a number of other QDs, such as InP, ZnSe, CuInS<sub>2</sub>, and lead halide perovskites, etc., have also been widely studied<sup>12–17</sup>, among which indium phosphide (InP)-based and zinc selenide (ZnSe)-based QDs are considered as promising benign alternatives, which are also capable of covering nearly the full range of natural colors<sup>3,18–24</sup>.

Up to this stage, Cd-free QLEDs still show inferior performance to those with Cd-based QLEDs. Nevertheless, having spent intense efforts in recent years, blue ZnSeTe and red InP QLEDs have a leaping advance. The optimized blue ZnSeTe QLED with double emitting layers showed an EQE of 20.2% close to the theoretical limit with a brightness of  $88,900 \text{ cd m}^{-2}$ <sup>25</sup>. In yet another approach, the red InP QLED has achieved an EQE of 21.4% with a high brightness of  $1.0 \times 10^5 \text{ cd m}^{-2}$ <sup>23</sup>. In comparison, the progress of InP-based green QLEDs still lags far behind. Under a conventional device structure that incorporates green InP/ZnSeS/ZnS QDs, a champion EQE of 13.6% was reported with a maximum luminance of  $13,900 \text{ (cd m}^{-2})$ <sup>26</sup>. As for a more practical inverted structure, the record high EQE for green InP QLEDs was even lower, which was reported to be 10.0% with a maximum luminance of  $4000 \text{ (cd m}^{-2})$ <sup>27</sup>. The inferior performance of green InP-based QLEDs mainly lies in the mismatched mobility between electron and hole. In the state-of-the-art organic/inorganic hybrid QLEDs, ZnO is commonly applied as an effective electron injection layer, rendering fast electron mobility<sup>26</sup>. Conversely, the hole injection is usually impeded due to the energy-level offset between emissive InP QDs and hole transporting layers. This leads to unbalanced electrons and holes in the recombining zone and hence low device efficiency<sup>2,6,28</sup>. Moreover, during the device operation, the excessive carriers accumulated at the barrier interface not only act as the non-radiative centers but also increase the driving voltage, limiting the device lifetime<sup>29–31</sup>. Theoretically, finding hole transport materials (HTMs) to match the energy levels of InP QDs is likely to improve hole injections, which unfortunately, is a great challenge because of the deep valence band of InP QDs<sup>32–34</sup>. Especially, theoretical approach on the energy-level alignments of a green InP/ZnSe/ZnS core/multi-shell structure indicates that the green InP QDs have a smaller  $e/h$  wave function overlap<sup>35</sup>, leading to further difficulty in adjusting the balance between electron and hole.

To circumvent the obstacle of electron/hole mismatch in green InP QLEDs, considerable efforts have been made to improve the energy-level alignment between the highest occupied molecular orbital (HOMO) of HTL and valence band of the InP QDs by

tailoring the shell structure of QDs<sup>7,36</sup>. These methods are, however, nontrivial, which must undergo modification by the synthesis of QDs multilayer structure. Alternatively, it may be more facile and effective to post-modify the structures of QDs, which may simultaneously minimize several impeding factors such as energy transfer, Auger recombination and/or charge accumulation at the interfaces, promoting the charge balance. In light of this, ligand exchange plays one of the keys, which is able to influence the carrier mobility by altering the inter-QD dielectric environment as well as the tunneling distance. It has been reported that the mobility can increase exponentially upon decreasing ligand length in the absence of any other modification<sup>37</sup>. Moreover, appropriate ligands can passivate electronic trap sites on the QD surface arising from the structural aperiodicity and/or off-stoichiometry of the QD core. This result may increase carrier and exciton lifetimes as well as provide a degree of control over the doping level and type of the coupled QD film<sup>38–40</sup>. Similar to the modification of the shell structure, altering the identity of the chemical binding group and dipole moment of the ligand should change the strength of the QD-ligand surface dipole, shifting the vacuum energy hence the valence band maximum (VBM) and conduction band minimum (CBM) of QDs. The influence of surface chemistry on the QD energy levels has been reported in a number of studies<sup>41–44</sup>.

The above modification, in theory, depends on the properties of the as-prepared InP QDs in terms of core/shell structure, original ligand passivation and importantly the emission quantum yield. The latter should be sufficiently high for the QLEDs performance, which is commonly inferior for InP QDs (cf. CdSe QDs). In this work, based on the green QDs (GQDs) of InP, that consistently exhibit high emission yield of  $86 \pm 2\%$  at 535 nm, we then performed post-modification of the QDs surface as well as interlayer modification of the energy levels. The key lies in the checks and balance of electron and hole mobility synergistically by post-passivation of the as-prepared InP GQDs. The systematic tuning brings closer the electron and hole mobility, resulting in a record high green InP QLED under an inverted device structure. Based on 30 devices being examined, an average EQE of 15.3% can be obtained, among which the champion EQE reaches 16.3% with the brightness of  $1.26 \times 10^4 \text{ cd m}^{-2}$  at 545 nm. Detail of results and discussion is elaborated in the following sections.

## Results and discussion

**Ligand-dependent properties.** For clarity, Fig. 1 depicts the progressive pathways to passivate the InP-based QDs. The as-prepared green InP/ZnSe/ZnS core/shell/shell QDs containing oleic acid ligands were measured to have an average diameter of  $\sim 8.6 \pm 1.2 \text{ nm}$ . These QDs, denoted as InP GQDs, consistently maintain their photoluminescence quantum yield (PLQY) of  $86 \pm 2\%$  (see Supplementary Fig. 1 for the detail of characterization). The resulted InP GQDs were further modified by the passivation of various alkyl diamines consisting of two amino groups, respectively, at two terminals bridged by various lengths of the alkyl chain. Note that one of the alkyl diamines, 1,2-ethylenediamine, used as a ligand, has been reported to boost the emission properties of CdTe/ZnS QDs by reducing the trapping site<sup>45</sup>. In addition to accommodate perhaps the trapping sites, the interaction of alkyl diamines with ZnS also has been reported to affect the ZnS structure, changing from cubic to hexagonal packing and hence altering the size of the particle to fine-tune the energy gap<sup>46</sup>. Similar alkyl diamines modification approach has not been explored in InP QDs. Due to the different lattice sizes and atom adduct properties, the exploitation of 1,2-

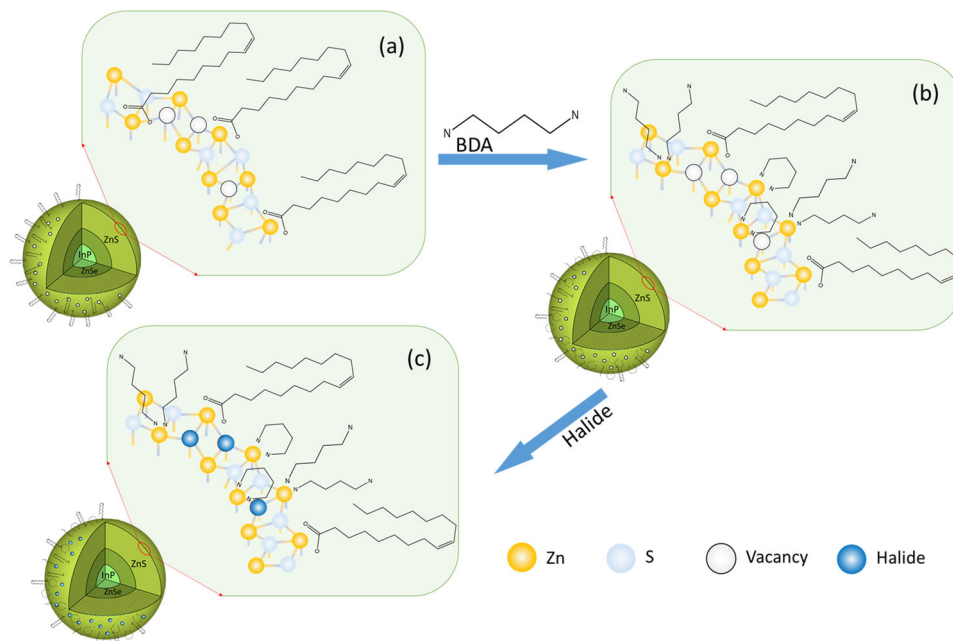


**Fig. 1** The schematic diagram of InP QDs passivated by the synergistic effect of BDA combined with zinc halides. **a** The as-prepared green InP/ZnSe/ZnS core/shell/shell QDs containing oleic acid ligands. **b** The resulted InP QDs were modified by the passivation of BDA consisting of two amino groups and **c** further modification by the passivation of various zinc halide additives.

ethylenediamine passivation in boosting CdTe/ZnS QDs may not work in InP QDs. In addition, as for various lengths of the alkyl chain, their insulation property may also largely affect the charge tunneling effect and hence the mobility. In this study, various alkyl diamines were selected and optimized via the performance of InP QLEDs where InP GQDs were modified by different alkyl diamines. As elaborated in the section of device fabrication it turned out that 1,4-butanediamine (BDA) rendered the top performance. Therefore, the results and discussion of the properties of post-modification are based on the BDA treated InP GQDs. The rest related data of the other alkyl diamines such as (1,2-ethylenediamine, EDA) and (1,6-hexanediamine, HDA) are listed and elaborated in the Supplementary Fig. 2.

Followed by the alkyl diamine (BDA) modification, further modification of InP GQDs were carried out by incorporating the halogen anions (Fig. 1). Addition of the halide salts to improve QDs optoelectronic performance has been reported in the case of CdSe/ZnS QDs<sup>47</sup>. Theoretical calculations have shown that the hole trapping sites originates from the coordination of chalcogenides on the surface of ZnS. Therefore, in theory, the small metal halide salts should be capable of filling the residual defects that BDA cannot accommodate<sup>48</sup>. Note that the optimization of zinc halides are mainly based on the performance of the corresponding QLED (vide infra). Among various zinc halide additives, it turns out that ZnI<sub>2</sub> added QLED exhibits the best device performance and will be the focus for the discussion. The rest related data of the other zinc halides such as ZnCl<sub>2</sub> and ZnBr<sub>2</sub> are listed and elaborated in the Supplementary Fig. 3.

**Optical measurements.** Figure 2a reveals the absorption spectra of the InP GQDs before and after passivation by BDA. Upon BDA passivation, non-negligibly, the absorption onset has been extended from 550 nm (2.25 eV) to 560 nm (2.21 eV). The decrease of bandgap after modification infers a number of possible combinations of the energy alignment between conduction band (CB) and valance band (VB). This is plausibly caused by

different degrees of CB and VB shift induced by the surface dipoles<sup>49</sup>, which, in theory, is an opportunity to block the electron injection but facilitate the hole injection. Further evidence of the bandgap change is given by the emission red shift from 535 to 540 nm in toluene upon BDA modification (see Fig. 2b). This BDA-modification-dependent luminescent peak wavelength in solution seems to be a disadvantage for later QLEDs application. However, upon fabrication into the device, it is interesting to know that the electroluminescence spectrum has negligible shift (<1 nm) between those with and without BDA-modified QDs devices (see Fig. 2c). This perhaps is due to the dominant dielectric interlayer environment that offsets the spectral changes in the device (vide infra). Further addition of metal halogen ions such as ZnCl<sub>2</sub>, ZnBr<sub>2</sub>, and ZnI<sub>2</sub> do not change the absorption and emission properties QDs (see Fig. 2a and b for the addition of ZnI<sub>2</sub>), implying that only rather small portion of trap sites remained after BDA modification. Nevertheless, due to the capping of the remaining trap sites at a large, the emission properties in terms of lifetime increase, as elaborated below.

The comparative studies were then made in the photoluminescence lifetime before and after the BDA modification; the corresponding data are listed in Table 1 (modification by other diamine and zinc halides, as shown in Supplementary Table 1). The time-resolved emission for the as-prepared and BDA-modified InP GQDs in toluene can be sufficiently fitted by two single exponential decay kinetics ( $\tau_1$ ,  $\tau_2$ ) of (19.5 ns, 68.6 ns) and (23.2 ns, 84.5 ns), respectively (see Fig. 2d and Table 1). Apparently, both  $\tau_1$  and  $\tau_2$  components increase with BDA post-modification. In general, the shorter  $\tau_1$  is related to a high rate of transition of interparticle charge and energy transfer, while the second exponent ( $\tau_2$ ) is attributed to charge carrier recombination<sup>50–53</sup>. The longer  $\tau_1$  and  $\tau_2$  observed in BDA-modified InP GQDs simply indicate less surface unfilled and oxidative defects, which is attributed to the uniform crystalline orientation on the QD surface<sup>48,54,55</sup>. The BDA modifying oxidation state of Zn in the InP GQDs is supported by XPS (see Supplementary Fig. 4), where the oxidation state of Zn is

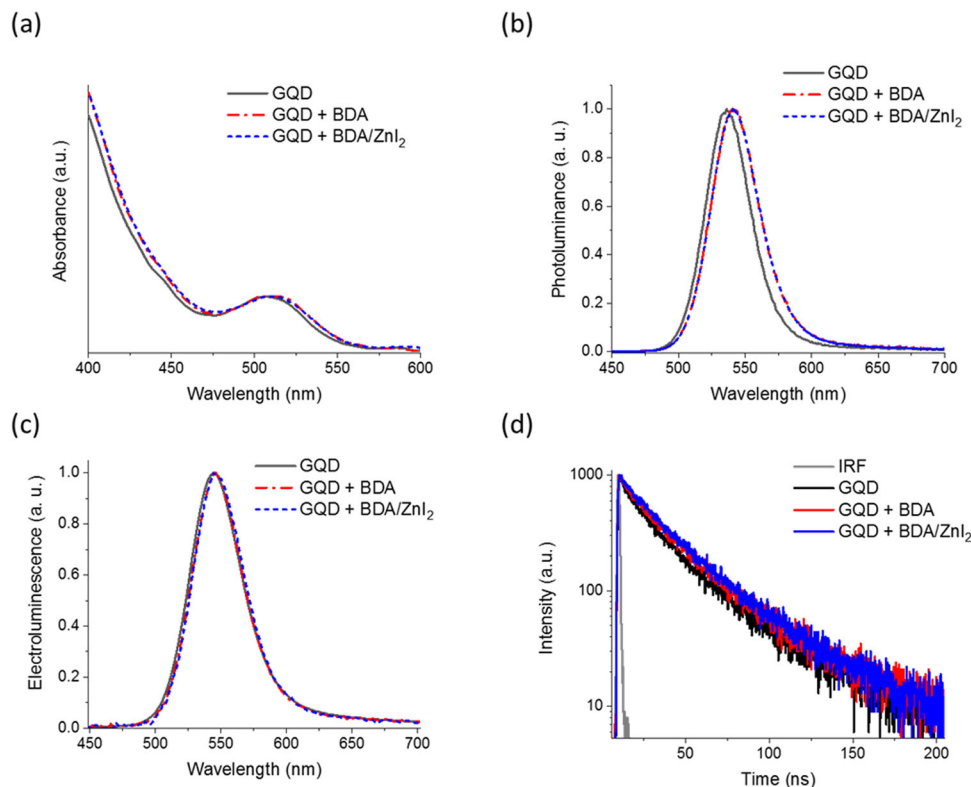


**Fig. 2 Optical properties of InP QDs.** **a** Absorption spectrum, **b** Photoluminescence spectrum, **c** Electroluminescence spectra at the same measuring condition (5 V), and **d** Photoluminescence decay of the InP QDs in toluene. The instrument response is shown by a solid gray line. The colors shown in the figure represent InP QDs before (black), after post-modification by BDA (red), and BDA followed by adding ZnI<sub>2</sub> (blue). The excitation wavelength for **b**, **c**, and **d** is at 400 nm.

**Table 1 The photoluminescence decay dynamics<sup>a</sup> of the as-prepared and post-modified InP QDs<sup>b</sup>.**

Post-modification	$a_1$	$\tau_1$ (ns)	$a_2$	$\tau_2$ (ns)	$\chi^2$
As prepared	0.86	19.5	0.14	68.6	1.18
BDA	0.89	23.2	0.11	84.5	1.33
BDA/ZnI <sub>2</sub>	0.90	25.8	0.10	85.5	1.07

<sup>a</sup>Lifetime was fitting by dual single exponential decay function:  $D(t) = a_1 \exp(-t/\tau_1) + a_2 \exp(-t/\tau_2)$  where  $a_1$  and  $a_2$  are the pre-exponential factors.

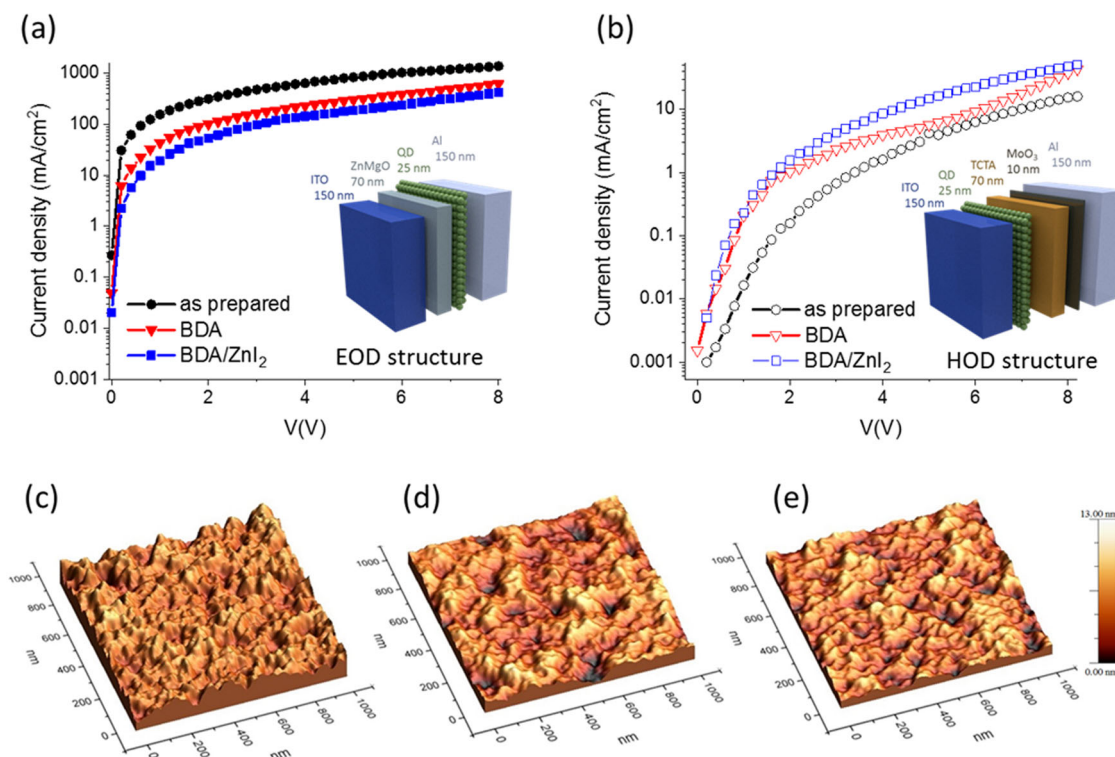
<sup>b</sup>The concentration for BDA and ZnI<sub>2</sub> was 0.4 and 0.125 mg ml<sup>-1</sup>, respectively.

reduced, rendering the evidence of less surface unfilled and oxidative defects. Upon adding ZnI<sub>2</sub> to the BDA-modified InP QDs, despite the unchanging of the absorption and emission spectral profile,  $\tau_1$  and  $\tau_2$  increase to 25.8, 85.5 ns, respectively, supporting the further suppression of the trapping sites.

**Device performance.** Prior to the device fabrication and performance, we firstly examined if the charge balancing has been improved by post-modification. This has been done by dividing the device structure into two parts, the electron-only and hole-only sections (Fig. 3a and b), and measured the current density for each site to correlate with the electron and hole mobility, respectively. Each part is mimicking half of the real device and the integration of these two parts exactly reproduces the whole device architecture elaborated later.

Figure 3a shows the current density versus voltage of the electron-only device (EOD). Apparently, in comparison to that of the as-prepared InP QDs, the BDA post-modified InP QDs effectively suppress the ability of electron injection. All other single post-modified processes are listed in the Supplementary Figs. 5 and 6 for comparison. The UPS data (see detailed description in Supplementary Fig. 7) suggests that the decrease of the electron mobility is due to the shift of vacuum level induced by the surface dipoles, resulting in the mismatch between the conduction band with the electron transport layer. Conversely, as mentioned early, the BDA post-modification decreases the hole trapping sites. As a result, the current density versus voltage of the hole-only device (HOD) reveals slight enhancement of the hole injection ability for the BDA-modified InP QDs (see Fig. 3b). Evidently, after BDA modification, the decrease of the electron mobility as opposed to the increase of the hole mobility makes more balance between electron and hole injection. Further improvement can be made by the BDA modification followed by the addition of zinc halides using ZnI<sub>2</sub> as the additive. The results shown in Fig. 3b reveal further increase of the hole injection mobility whereas the change of electron mobility is not as significant. This may be rationalized, on the one hand, by the additional filling of vacancies by the zinc iodide salt, further reducing the hole traps<sup>56</sup>. On the other hand, the weak surface interaction as well as relatively small amount of the passivated iodide does not change the surface dipole and hence the band levels remain relatively unchanged (cf. the BDA modification only). We also noticed that the film morphology of InP QDs has been improved accordingly via sequence of passivation. Figure 3c–e shows the atomic force microscope (AFM) height





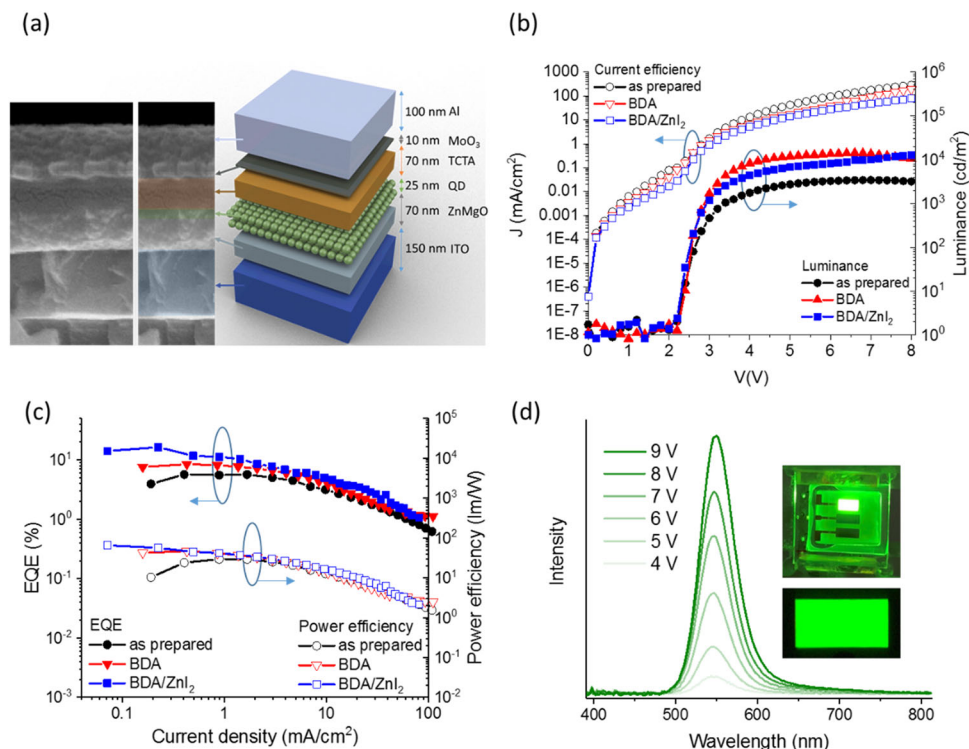
**Fig. 3 Characterization of single-carrier devices and AFM images.** The current density-voltage profiles of the **a** electron-only devices and **b** hole-only devices with the as prepared (black), BDA modified (red) and BDA followed by ZnI<sub>2</sub> passivated (blue) InP QDs. The inserts show the schematic diagram of electron and hole-only device structures. Also shown are the AFM height images of the same scanned area for **c** as prepared, **d** BDA modified and **e** BDA followed by ZnI<sub>2</sub> passivated InP QDs films.

image of the same scanned area for the as-prepared InP QDs film (RMS roughness 1.63 nm), BDA-modified film (RMS roughness 1.39 nm), and BDA followed by ZnI<sub>2</sub> passivated film (RMS roughness 1.17 nm). Because BDA with double end NH<sub>2</sub> can both anchor Zn on the InP QD surface, it provides an opportunity to bridge the nearby QDs, stabilizing the film formation. Accordingly, we speculate that the decrease in RMS is related to some BDA bound to the proximal QDs on the surface. The decrease of RMS roughness along the sequence of BDA and then ZnI<sub>2</sub> modification manifests the improvement of the surface smoothness and hence suppression of the leakage current.

Figure 4a shows the schematic diagram of the InP QDs device structure applied in this study. Also depicted in Fig. 4a are the cross-sectional SEM images of the interlayer configuration. Note that the electron transport layer consists of Zn<sub>x</sub>Mg<sub>1-x</sub>O where Mg has been finely-tuned to 12.5% for the optimized performance. Table 2 systematically lists the device performance data for the as prepared, BDA and other alkyl diamines modified as well as the combination of BDA and zinc halides modified InP QDs QLEDs. For each condition, data shown in Table 2 are the average value of a number of devices fabricated. Comprehensive data of all measured devices are listed in Supplementary Table 2 where several checking points can be pointed out here. First, among various alkyl diamines-modified InP QDs devices, the ethylene 1,2-diamine (EDA)-modified InP QDs devices has already shown better performance than that of the unmodified InP QDs device. For example, typical device performance indices such as maximum external quantum efficiency (EQE<sub>max</sub>) and maximum current efficiency (CE<sub>max</sub>) for EDA modified InP QDs, measured to be 7.9% and 35.9 cd A<sup>-1</sup>, respectively, are higher than that (5.7% and 27.9 cd A<sup>-1</sup>) of the unmodified InP QDs device. Upon increasing the alkyl lengths of diamines from

none, EDA, BDA to HDA, both CE<sub>max</sub> and external EQE<sub>max</sub> exhibit a volcano shape-like plot, reaching the pinnacle at BDA-modified InP QLED with CE<sub>max</sub> and EQE<sub>max</sub> of 44.3 cd A<sup>-1</sup> and 8.5%, respectively (see Table 2). Therefore, BDA with four carbon bridging lengths seems to be optimum for filling the trap sites as well as for tuning the electron/hole balance, consistent with the results of charge mobility measured in the electron and hole-only section of the device (vide supra). Upon further increasing the ligand length to six carbon atoms, i.e., the HDA, the long spatial distance between two terminal amines increases the structure variance, which is unfavorable for the diamino-chelation onto the surface of QDs. This, together with the increase of the hydrophobic/insulation to suppress the charge injection, leads to the inferiority in device performance, being dropping to only 14.4 cd A<sup>-1</sup> and 1.8% for CE<sub>max</sub> and EQE<sub>max</sub>, respectively. Supplementary Table 2 lists other performance data such as CE, PE, and EQE at 1000 cd m<sup>-2</sup>.

Based on the BDA-modified InP QDs, we then move one step further by additionally passivating zinc halides to examine if the BDA/zinc halides modified InP QDs can further improve the QLED properties. Note that more balanced electron/hole mobility has been proved by the current density versus voltage of the electron and hole-only device individually (see Fig. 3). Even though the devices show similar performance by passivation of different zinc halides (see Supplementary Table 2), ZnI<sub>2</sub> shown better solubility and hence better device efficiency upon combining BDA, which is supposed to be a synergistic effect. For a fair comparison, the best device performance for BDA/ZnI<sub>2</sub> passivated InP QDs are depicted in Fig. 4b and c with corresponding data listed in Table 2. Apparently, the BDA/ZnI<sub>2</sub> passivated InP QDs make leap advance in either the current density and luminescence versus the applied voltage or the



**Fig. 4** The characteristics of InP-based QLEDs. **a** The SEM image of the interlayers cross section and corresponding device structure. Note that right part of the SEM image has been intentionally colored to show clear correlation with the device structure. **b** The plot of current density (left axis) and luminance (right axis) versus the applied voltage, **c** EQE (left axis) and power efficiency (right axis) versus current density profiles. Performances of as prepared (black), BDA modified (red), and BDA followed by ZnI<sub>2</sub> passivated (blue) InP-based QLEDs. **d** The voltage-dependent electroluminescent spectra of the QLED with BDA/ZnI<sub>2</sub> modification. Inset: photographs of the operating devices.

**Table 2** Performances of the QLEDs of the as-prepared and post-modified InP QDs where the concentration 0.4 and 0.125 mg ml<sup>-1</sup> was added for various zinc halides and alkyl diamines, respectively.

Post-modification	L <sub>max</sub> [cd m <sup>-2</sup> ]	CE <sub>max</sub> [cd A <sup>-1</sup> ]	PE <sub>max</sub> [lm W <sup>-1</sup> ]	EQE <sub>max</sub> [%]
As prepared	3427.7	27.9	29.4	5.7
EDA	13,756.1	35.9	43.8	7.9
BDA	14,287.6	44.3	46.4	8.5
HAD	7879.2	14.4	17.4	1.8
BDA/ZnCl <sub>2</sub>	9182.3	53.8	65.0	13.5
BDA/ZnBr <sub>2</sub>	11,853.5	41.2	46.2	15.2
BDA/ZnI <sub>2</sub>	12,646.3	57.5	56.4	16.3

current efficiency and EQE versus current density. Having fabricated 30 devices where InP QDs are passivated by BDA, followed by ZnI<sub>2</sub> addition (0.125 mg, see Supplementary Fig. 8 for detail), the average CE<sub>max</sub> and EQE<sub>max</sub> are as high as 45.5 ± 5.5 cd A<sup>-1</sup> and 15.3 ± 1.0%. The champion one gives CE<sub>max</sub> and EQE<sub>max</sub> of 57.5 cd A<sup>-1</sup> and 16.3%, respectively.

We also examined the device performance of adding other zinc halides additives such as ZnCl<sub>2</sub> and ZnBr<sub>2</sub> to the BDA-modified InP QDs. The resulted data listed in Table 2 and Supplementary Table 2 all show better performance than that of the BDA modified only InP QLED. Nevertheless, champion performance still belongs to that of BDA/ZnI<sub>2</sub> passivated green InP QLED. It is also noteworthy that emission quantum yield of InP QLED is within 86%. Taking the internal quantum efficiency of 100% and

1/5 of all solid angles covered, a theoretically limited EQE of 17.2% can reach. The champion device of EQE 16.3% is thus close to the theoretical limit. The device also achieves a brightness of 1.26 × 10<sup>4</sup> cd m<sup>-2</sup> under a bias of 8.8 V. Figure 5 highlights the systematic improvement in each stage, where the performance of devices treated by BDA/ZnI<sub>2</sub> modification process is clearly better than those of the BDA modified only and the as-prepared ones. As the modification process progresses, the EQE is increasing with the current density of HOD, and decreasing with current density of EOD. Other devices performances shown in Fig. 5, including L<sub>max</sub>, CE<sub>max</sub>, and PE<sub>max</sub>, also reveal superiority to those of the as-prepared one.

**Comparison of green QD-LEDs.** We then fairly compare the above results with those of the reported green InP QLEDs up to this stage. The corresponding data listed in Table 3 clearly manifest the breakthrough of the device performance in this work. Under the same inverted device structure, this work shows leaping enhancement, in which CE<sub>max</sub>, PE<sub>max</sub>, and EQE are more than 12 folds, 13 folds, and 1.6 times better than those of the previous best data reported for each single parameter. Further extension to all InP QDs relevant devices, including those of the conventional structures, the current device renders the same level of PE<sub>max</sub> and luminance, but apparently is superior in terms of the lowest turn-on voltage of 2.2 V, the highest EQE of 16.3% and highest CE<sub>max</sub> of 57.5 cd A<sup>-1</sup>.

Last but not the least, in this study we also carried out the device lifetime measurements to gain further insight into the relationship between electroluminescence efficiency and stability. To our knowledge, there is no practical and meaningful report in regards to the lifetime of the green-emitting InP-based QD-LEDs. Figure 6

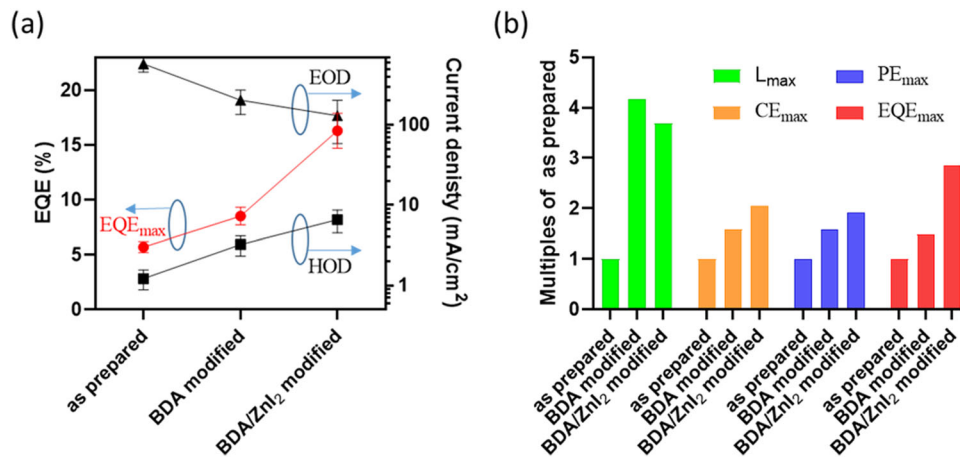


**Fig. 5** The comparison among as-prepared, BDA-modified, and BDA/ZnI<sub>2</sub>-modified InP QD devices. **a** The EQE (red circle) increases in HOD (black square) and decreases in EOD (black triangle) upon increasing the current density. The error bars show standard deviation of as prepared for  $n = 5$ , BDA modified for  $n = 10$ , and BDA/ZnI<sub>2</sub> modified for  $n = 30$ , respectively. **b** The relative multiples with respect to the as-prepared device for  $L_{\max}$ ,  $CE_{\max}$ ,  $PE_{\max}$ , and  $EQE_{\max}$ .

shows the evolution of electroluminescence intensities and other parameters for the InP QD devices operating over a period of 4 h at an initial luminance of  $2000 \text{ cd m}^{-2}$ . Also, the  $T_{50}$  value at  $100 \text{ cd m}^{-2}$  was estimated by fitting the data with an empirical equation  $L^n \times T_{50} = \text{constant}$ , where  $L$  is the initial luminance and  $n$  is the acceleration factor that was determined by fitting the data shown in Supplementary Fig. 9. As a result,  $T_{50}$  at  $100 \text{ cd m}^{-2}$  increases from 373.9 to 545.8 h upon BDA modification. After BDA/ZnI<sub>2</sub> modification,  $T_{50}$  at  $100 \text{ cd m}^{-2}$  lifts significantly to 1033.4 h. We must admit that the relatively crude packaging system currently existing in the lab cannot satisfy the rigorous lifetime test. Nevertheless, the trend of systematic increase of the device lifespan makes promising the superiority of BDA/ZnI<sub>2</sub> modification in addition to the record high performance in device efficiency.

## Conclusion

In summary, we have carried out extensive post-modification of the colloidal green InP QDs by a sequence of ligand exchanges with various alkyl diamines and zinc halides. Our goal is to balance the electron and hole mobility and hence to promote the corresponding QLED performance. The alkyl diamines ligation provides bifunctionality, where upon surface passivation both energy level of CB and VB of InP QDs lift due to the interface dipole interaction, facilitating the hole mobility, whereas the electron injection is retarded. In addition, the passivation fills the hole trapping sites as well as smoothens the surface of the film. Accommodation of the hole trapping site can be further suppressed by adding zinc halides, such that the InP QDs and the corresponding QLEDs can be shaped up to the optimal condition. The comprehensive test of alkyl diamines and zinc halides turns out that BDA and ZnI<sub>2</sub> are the optimized combination to balance the electron/hole mobility and hence to maximize the performance of the green InP QLEDs. With 30 devices being fabricated, the record high average EQE of  $15.3 \pm 1.0\%$  has been reached, among which the maximum EQE 16.3% has approached nearly the theoretical limit of the currently prepared InP QDs, having an emission quantum yield of 86%. This work thus offers a general guideline where passivation of green InP QDs can in principle harness the device efficiency without altering the device structures, facilitating the green InP QLEDs to play a key role in full-color displays.

## Methods

**Chemicals.** Zinc acetate dehydrate (99%) and dimethyl sulfoxide (DMSO, 99.9%) were purchased from J.T. Baker. Tetramethylammonium hydroxide pentahydrate

(TMAH, 97%), magnesium acetate tetrahydrate (99%), ethanol (anhydrous, 99.8%), and 1,6-hexanediamine (HDA, 98%) were purchased from Sigma-Aldrich. Toluene (99.85%), 2-methoxyethanol (2MoE, 99%), and zinc iodide (98%) were purchased from Acros organics. 1,2-Ethylenediamine (EDA, 99%), 1,4-Butanediamine (BDA, 98%), zinc chloride (98%), zinc bromide (98%), and molybdenum (VI) oxide (MoO<sub>3</sub>, 99.95%) were purchased from Alfa Aesar. Tris(4-carbazoyl-9-ylphenyl)amine (TCTA) was purchased from Shine Materials Technology. The passivation process was carried out by mixing EDA, BDA or HAD toluene solution ( $8 \text{ mg ml}^{-1}$ ) and solution of ZnCl<sub>2</sub>, ZnBr<sub>2</sub>, and ZnI<sub>2</sub> anhydrous ethanol solution ( $2.5 \text{ mg ml}^{-1}$ ) in a 1:1 ratio by volume. Alternatively, if only diamine is used for the passivation, then adding solely anhydrous ethanol should be an optimum process. The prepared stock solution ( $0.1 \text{ ml}$ ) was then mixed with InP QDs ( $10 \text{ mg}$ ) in toluene ( $1 \text{ ml}$ ) to reach the desired concentration. Based on this protocol, we have reported a facile and efficient method where there is no need to carry out further purification process. Green InP/ZnSe/ZnS QDs with a diameter around  $8.6 \pm 1.2 \text{ nm}$  were supported by Unique Materials Co., Ltd. and measured by TEM as shown in Supplementary Fig. 1.

**Preparation of ZnMgO with Mg 12.5 mol% nanoparticles.** Colloidal ZnMgO nanoparticles were synthesized as following a published method with some modifications<sup>17</sup>. Zn(AC)<sub>2</sub>·2H<sub>2</sub>O (8.75 mmole) and Mg(AC)<sub>2</sub>·4H<sub>2</sub>O (1.25 mmole) were dissolved in 40 ml of DMSO solution. twenty milliliters of ethanol containing 7.5 mmole tetramethylammonium hydroxide (TMAH) solution were added dropwise into the Zn/Mg acetate solution at  $0.5 \text{ ml min}^{-1}$  and the mixture was vigorously stirred for 30 min. ZnMgO nanoparticles were then precipitated by adding ethyl acetate and centrifugation at 8000 r.p.m for 3 min. The precipitation was redispersed in 2-methoxyethanol contain with 50  $\mu\text{l}$  of ethanolamine to stabilize the solution, and then stored in the fridge.

**Device fabrication.** The ITO/glass substrates were ultrasonically cleaned with deionized water, acetone, and IPA for 20 min, respectively. The ZnMgO nanoparticle solution was then spin-coated onto the ITO/glass substrates at 2500 r.p.m. for 50 s and baked at  $185 \text{ }^\circ\text{C}$  for 30 min. Post-modified QDs as mentioned above dispersions in toluene ( $10 \text{ mg ml}^{-1}$ ) were spin-coated onto the ZnMgO layer at 3000 rpm for 50 s and then baking at  $150 \text{ }^\circ\text{C}$  for 20 min. TCTA, MoOx and Al electrodes were deposited using a thermal evaporation system through shadow masks under a high vacuum ( $<10^{-5} \text{ Pa}$ ). The active device areas were  $10 \text{ mm}^2$  and measured with encapsulation. The final surface ligands exchange percentages were identified and quantified by FTIR, TGA, and XPS experiments shown in Supplementary Figs. 10–12 and Supplementary Table 3, see Supplementary Note 1.

**Characterization.** Absorption and PL spectra of QDs were recorded by Hitachi U-3310 spectrophotometer and Edinburgh FS980 fluorimeter, respectively. The emission quantum yield of InP QDs was measured by a diluted InP QDs in the toluene where the absorbance at the excitation wavelength (e.g., 450 nm) no more than 0.1 to avoid reabsorption. The integrated emission intensity was then compared with the standard Rhodamine 6 G in EtOH where the quantum yield of the 552 nm emission band was reported to be 95%. The PLQY is then calculated by following equation.

$$Q_S = Q_R \frac{I_S A_R n_S^2}{I_R A_S n_R^2}$$



Table 3 Major progress of the InP green QDs-based QLEDs.

Device structure	QD structure	V <sub>on</sub> (V)	L (cd m <sup>-2</sup> )	CE <sub>max</sub> (cd A <sup>-1</sup> )	PF <sub>max</sub> (lm W <sup>-1</sup> )	EQE <sub>max</sub> (%)	EL (nm)	PL (nm)	PL FWHM (nm)	PLQY (%)	reference
Inverted	InP/ZnSeS/ZnS	2.2	12,646	57.5	56.4	16.3	545	535	39	86	This work
	InP/ZnSeS/ZnS	2.2	10,490	4.44	4.32	1.5	545	525	65		2017, Small <sup>19</sup> , 2020, Appl. Phys. Lett <sup>27</sup> , 2021, Adv. Funct. Mater <sup>57</sup> , 2019, Advanced Optical Materials <sup>22</sup> , 2019, Chem. Commun <sup>26</sup> , 2021, Mater Electron <sup>58</sup> .
	QDA524-100 (Merck)	2.4	~4000			10	530		45	95	
Normal	InP/ZnSeS/ZnS		1836			7.06	525				
	InP/GaP/ZnS//ZnS		2938	13.7		6.3	530	527	58	70	
	InP based	2.5	13,900		69.5	13.6		531	34	82	
	InP@ZnSeS/ZnS			4.79		1.68		518	46	67.5	

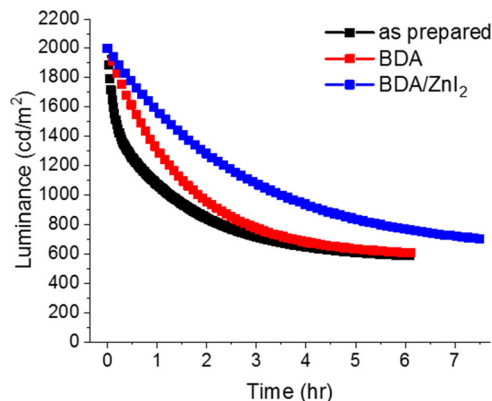


**Fig. 6 Lifetime measurements.** Operational lifetimes of QGD-LEDs under a condition of 2000 cd m<sup>-2</sup> for the as-prepared InP QDs QLEDs (black) as well as the BDA (red) as BDA/ZnI<sub>2</sub> (blue) modified InP QDs QLEDs.

Where  $Q_S$  is the quantum yield of an unknown fluorescent sample and  $Q_R$  is the quantum yield of the reference standard. Here,  $I_S$  and  $I_R$  are the integrated fluorescence intensities for the unknown and reference samples, respectively, while  $A_S$  and  $A_R$  are the respective absorbance values of the unknown and reference samples;  $n_S$  and  $n_R$  are the refractive indices of the unknown and reference samples.

Cross-sectional scanning transmission electron microscopy (SEM) images were performed using a Hitachi S-4800 field emission scanning electron microscope. Atomic force microscopy (AFM) measurements were conducted on a Utek Material Nanoview 1000 with tapping mode at ambient temperature. The current density – voltage – luminance (J–V–L) and current efficiency–external quantum efficiency–luminance (CE–EQE–L) characteristics were characterized by a CR-280 spectrometer equipped with a source meter (Keithley 2400).

#### Data availability

Main data supporting the findings of this study are contained within the paper and its associated Supplementary Information. All relevant data of this study are available from the corresponding authors upon reasonable request.

Received: 19 May 2021; Accepted: 1 September 2021;

Published online: 17 September 2021

#### References

- Qian, L., Zheng, Y., Xue, J. & Holloway, P. H. Stable and efficient quantum-dot light-emitting diodes based on solution-processed multilayer structures. *Nat. Photonics* **5**, 543–548 (2011).
- Mashford, B. S. et al. High-efficiency quantum-dot light-emitting devices with enhanced charge injection. *Nat. Photonics* **7**, 407–412 (2013).
- Moon, H., Lee, C., Lee, W., Kim, J. & Chae, H. Stability of quantum dots, quantum dot films, and quantum dot light-emitting diodes for display applications. *Adv. Mater.* **31**, 1804294 (2019).
- Kim, D. et al. Polyethylenimine ethoxylated-mediated all-solution-processed high-performance flexible inverted quantum dot-light-emitting device. *ACS Nano* **11**, 1982–1990 (2017).
- Colvin, V. L., Schlamp, M. C. & Alivisatos, A. P. Light-emitting diodes made from cadmium selenide nanocrystals and a semiconducting polymer. *Nature* **370**, 354–357 (1994).
- Dai, X. et al. Solution-processed, high-performance light-emitting diodes based on quantum dots. *Nature* **515**, 96–99 (2014).
- Shen, H. et al. Visible quantum dot light-emitting diodes with simultaneous high brightness and efficiency. *Nat. Photonics* **13**, 192–197 (2019).
- Sun, Y. et al. Investigation on thermally induced efficiency roll-off: toward efficient and ultrabright quantum-dot light-emitting diodes. *ACS Nano* **13**, 11433–11442 (2019).
- Fu, Y., Jiang, W., Kim, D., Lee, W. & Chae, H. Highly efficient and fully solution-processed inverted light-emitting diodes with charge control interlayers. *ACS Appl. Mater. Interfaces* **10**, 17295–17300 (2018).
- Wang, L. et al. Blue quantum dot light-emitting diodes with high electroluminescence efficiency. *ACS Appl. Mater. Interfaces* **9**, 38755–38760 (2017).
- Yuan, Q. et al. A review on the electroluminescence properties of quantum-dot light-emitting diodes. *Org. Electron.* **90**, 106086 (2021).
- Kim, J.-H. & Yang, H. High-efficiency Cu-In-S quantum-dot-light-emitting device exceeding 7%. *Chem. Mater.* **28**, 6329–6335 (2016).



13. Bai, Z. et al. Hydroxyl-terminated CuInS<sub>2</sub> based quantum dots: toward efficient and bright light emitting diodes. *Chem. Mater.* **28**, 1085–1091 (2016).
14. Lin, K. et al. Perovskite light-emitting diodes with external quantum efficiency exceeding 20 per cent. *Nature* **562**, 245–248 (2018).
15. Liu, Y. et al. Efficient blue light-emitting diodes based on quantum-confined bromide perovskite nanostructures. *Nat. Photonics* **13**, 760–764 (2019).
16. Jia, Y.-H. et al. Role of excess FAI in formation of high-efficiency FAPbI<sub>3</sub>-based light-emitting diodes. *Adv. Funct. Mater.* **30**, 1906875 (2020).
17. Kim, J.-H. et al. Performance improvement of quantum dot-light-emitting diodes enabled by an alloyed ZnMgO nanoparticle electron transport layer. *Chem. Mater.* **27**, 197–204 (2015).
18. Lim, J. et al. Highly efficient cadmium-free quantum dot light-emitting diodes enabled by the direct formation of excitons within InP@ZnSeS quantum dots. *ACS Nano* **7**, 9019–9026 (2013).
19. Wang, H. C. et al. Cadmium-free InP/ZnSeS/ZnS heterostructure-based quantum dot light-emitting diodes with a ZnMgO electron transport layer and a brightness of over 10 000 cd m<sup>-2</sup>. *Small* **13**, 1603962 (2017).
20. Hahn, D. et al. Design principle for bright, robust, and color-pure InP/ZnSe<sub>x</sub>S<sub>1-x</sub>/ZnS heterostructures. *Chem. Mater.* **31**, 3476–3484 (2019).
21. Lee, C. Y. et al. Efficient cadmium-free inverted red quantum dot light-emitting diodes. *ACS Appl. Mater. Interfaces* **11**, 36917–36924 (2019).
22. Zhang, H. et al. High-efficiency green InP quantum dot-based electroluminescent device comprising thick-shell quantum dots. *Adv. Opt. Mater.* **7**, 1801602 (2019).
23. Won, Y.-H. et al. Highly efficient and stable InP/ZnSe/ZnS quantum dot light-emitting diodes. *Nature* **575**, 634–638 (2019).
24. Li, Y. et al. Stoichiometry-controlled InP-based quantum dots: synthesis, photoluminescence, and electroluminescence. *J. Am. Chem. Soc.* **141**, 6448–6452 (2019).
25. Kim, T. et al. Efficient and stable blue quantum dot light-emitting diode. *Nature* **586**, 385–389 (2020).
26. Moon, H. et al. Composition-tailored ZnMgO nanoparticles for electron transport layers of highly efficient and bright InP-based quantum dot light emitting diodes. *Chem. Commun.* **55**, 13299–13302 (2019).
27. Iwasaki, Y., Motomura, G., Ogura, K. & Tsuzuki, T. Efficient green InP quantum dot light-emitting diodes using suitable organic electron-transporting materials. *Appl. Phys. Lett.* **117**, 111104 (2020).
28. Yang, Y. et al. High-efficiency light-emitting devices based on quantum dots with tailored nanostructures. *Nat. Photonics* **9**, 259–266 (2015).
29. So, F. & Kondakov, D. Degradation mechanisms in small-molecule and polymer organic light-emitting diodes. *Adv. Mater.* **22**, 3762–3777 (2010).
30. Chen, S., Jiang, X. & So, F. Hole injection polymer effect on degradation of organic light-emitting diodes. *Org. Electron.* **14**, 2518–2522 (2013).
31. Coburn, C. & Forrest, S. R. Effects of charge balance and exciton confinement on the operational lifetime of blue phosphorescent organic light-emitting diodes. *Phys. Rev. Appl.* **7**, 041002 (2017).
32. Caruge, J. M., Halpert, J. E., Wood, V., Bulović, V. & Bawendi, M. G. Colloidal quantum-dot light-emitting diodes with metal-oxide charge transport layers. *Nat. Photonics* **2**, 247–250 (2008).
33. Kwak, J. et al. Bright and efficient full-color colloidal quantum dot light-emitting diodes using an inverted device structure. *Nano Lett.* **12**, 2362–2366 (2012).
34. Bai, L. et al. A quinoxaline based N-heteroacene interfacial layer for efficient hole-injection in quantum dot light-emitting diodes. *Nanoscale* **7**, 11531–11535 (2015).
35. Jang, E., Kim, Y., Won, Y.-H., Jang, H. & Choi, S.-M. Environmentally friendly InP-based quantum dots for efficient wide color gamut displays. *ACS Energy Lett.* **5**, 1316–1327 (2020).
36. Cao, W. et al. Highly stable QLEDs with improved hole injection via quantum dot structure tailoring. *Nat. Commun.* **9**, 2608 (2018).
37. Liu, Y. et al. Dependence of carrier mobility on nanocrystal size and ligand length in PbSe nanocrystal solids. *Nano Lett.* **10**, 1960–1969 (2010).
38. Voznyy, O. et al. A charge-orbital balance picture of doping in colloidal quantum dot solids. *ACS Nano* **6**, 8448–8455 (2012).
39. Oh, S. J. et al. Stoichiometric control of lead chalcogenide nanocrystal solids to enhance their electronic and optoelectronic device performance. *ACS Nano* **7**, 2413–2421 (2013).
40. Kim, D., Kim, D. H., Lee, J. H. & Grossman, J. C. Impact of stoichiometry on the electronic structure of PbS quantum dots. *Phys. Rev. Lett.* **110**, 196802 (2013).
41. Soreni-Harari, M. et al. Tuning energetic levels in nanocrystal quantum dots through surface manipulations. *Nano Lett.* **8**, 678–684 (2008).
42. Timp, B. A. & Zhu, X. Y. Electronic energy alignment at the PbSe quantum dots/ZnO(10 $\bar{1}$ 0) interface. *Surf. Sci.* **604**, 1335–1341 (2010).
43. Jasieniak, J., Califano, M. & Watkins, S. E. Size-dependent valence and conduction band-edge energies of semiconductor nanocrystals. *ACS Nano* **5**, 5888–5902 (2011).
44. Munro, A. M., Zacher, B., Graham, A. & Armstrong, N. R. Photoemission spectroscopy of tethered CdSe nanocrystals: shifts in ionization potential and local vacuum level as a function of nanocrystal capping ligand. *ACS Appl. Mater. Interfaces* **2**, 863–869 (2010).
45. Mandal, A. & Tamai, N. Suppressed blinking behavior of thioglycolic acid capped CdTe quantum dot by amine functionalization. *Appl. Phys. Lett.* **99**, 263111 (2011).
46. Pattnaik, A., Tomar, M., Gupta, V., Prasad, B. & Mondal, S. Optical study of ZnS nano spheres with varying amount of ethylenediamine for photovoltaic application. *Integr. Ferroelectr.* **194**, 135–144 (2018).
47. Kang, B.-H. et al. Efficient exciton generation in atomic passivated CdSe/ZnS quantum dots light-emitting devices. *Sci. Rep.* **6**, 34659 (2016).
48. Chiang, C.-H. & Wu, C.-G. A method for the preparation of highly oriented MAPbI<sub>3</sub> crystallites for high-efficiency perovskite solar cells to achieve an 86% fill factor. *ACS Nano* **12**, 10355–10364 (2018).
49. Jinnouchi, R., Akimov, A. V., Shirai, S., Asahi, R. & Prezhdo, O. V. Upward shift in conduction band of Ta<sub>2</sub>O<sub>5</sub> due to surface dipoles induced by N-doping. *J. Phys. Chem. C* **119**, 26925–26936 (2015).
50. Cho, Y. et al. Balancing charge carrier transport in a quantum dot P-N junction toward hysteresis-free high-performance solar cells. *ACS Energy Lett.* **3**, 1036–1043 (2018).
51. Choi, M. K. et al. Extremely vivid, highly transparent, and ultrathin quantum dot light-emitting diodes. *Adv. Mater.* **30**, 1703279 (2018).
52. Cao, F. et al. High-efficiency, solution-processed white quantum dot light-emitting diodes with serially stacked red/green/blue units. *Adv. Opt. Mater.* **6**, 1800652 (2018).
53. Su, Q., Sun, Y., Zhang, H. & Chen, S. Origin of positive aging in quantum-dot light-emitting diodes. *Adv. Sci.* **5**, 1800549 (2018).
54. Kamminga, M. E. et al. Micropatterned 2D hybrid perovskite thin films with enhanced photoluminescence lifetimes. *ACS Appl. Mater. Interfaces* **10**, 12878–12885 (2018).
55. Zeng, Q. et al. Polymer-passivated inorganic cesium lead mixed-halide perovskites for stable and efficient solar cells with high open-circuit voltage over 1.3 V. *Adv. Mater.* **30**, 1705393 (2018).
56. Houtepen, A. J., Hens, Z., Owen, J. S. & Infante, I. On the origin of surface traps in colloidal II-VI semiconductor nanocrystals. *Chem. Mater.* **29**, 752–761 (2017).
57. Liu, P. et al. Green InP/ZnSeS/ZnS core multi-shelled quantum dots synthesized with aminophosphine for effective display applications. *Adv. Funct. Mater.* **31**, 2008453 (2021).
58. Jiang, W., Choi, Y. & Chae, H. Efficient green indium phosphide quantum dots with tris(dimethylamino)-phosphine phosphorus precursor for electroluminescent devices. *J. Mater. Sci. Mater. El.* **32**, 4686–4694 (2021).

## Acknowledgements

This work was supported by the Ministry of Science and Technology, Taiwan, for financial support. We Thank for the TGA data from Thermal Analysis System of Instrumentation Center, National Taiwan University. We acknowledge the technical support provided by the Center for Emergent Materials and Advanced Devices, National Taiwan University.

## Author contributions

W.C.C. conceived the work. T.H.C. manufactured the samples. Y.C.L. performed SEM measurements on the sample. Z.X.H. performed experimental AFM measurements. C.H.C. performed electrical measurements and assist QDEL device production. C.C.L. assist in the coordination of InP QD synthesis. C.H.W. performed the FTIR measurement. H.W.T. performed InP QDs design of the structures. W.Y.H. performed device lifetime measurements. P.T.C. drafted the manuscript, with contributions from all authors in editing and revision stages.

## Competing interests

The authors declare no competing interests.

## Additional information

**Supplementary information** The online version contains supplementary material available at <https://doi.org/10.1038/s43246-021-00203-5>.

**Correspondence** and requests for materials should be addressed to Huan-Wei Tseng, Wen-Yi Hung or Pi-Tai Chou.

**Peer review information** *Communications Materials* thanks Huaibin Shen and the other, anonymous, reviewer(s) for their contribution to the peer review of this work. Primary Handling Editor: John Plummer.

**Reprints and permission information** is available at <http://www.nature.com/reprints>

**Publisher's note** Springer Nature remains neutral with regard to jurisdictional claims in published maps and institutional affiliations.



**Open Access** This article is licensed under a Creative Commons Attribution 4.0 International License, which permits use, sharing, adaptation, distribution and reproduction in any medium or format, as long as you give appropriate credit to the original author(s) and the source, provide a link to the Creative Commons license, and indicate if changes were made. The images or other third party material in this article are included in the article's Creative Commons license, unless indicated otherwise in a credit line to the material. If material is not included in the article's Creative Commons license and your intended use is not permitted by statutory regulation or exceeds the permitted use, you will need to obtain permission directly from the copyright holder. To view a copy of this license, visit <http://creativecommons.org/licenses/by/4.0/>.

© The Author(s) 2021